

Supporting information
for:

Mixed-Valence Nickel-Iron Dithiolates Related to the [NiFe]-Hydrogenases

David Schilter, Mark J. Nilges, Mrinmoy Chakrabarti, Paul A. Lindahl, Thomas B. Rauchfuss, Matthias Stein

^aDepartment of Chemistry, University of Illinois, 600 S. Goodwin Ave.
Urbana, IL 61801

^bDepartment of Chemistry, Texas A&M University,
College Station, TX 77842-3012

^cMax Planck Institute for Dynamics of Complex Technical Systems, Sandtorstraße 1,
39106 Magdeburg, Germany

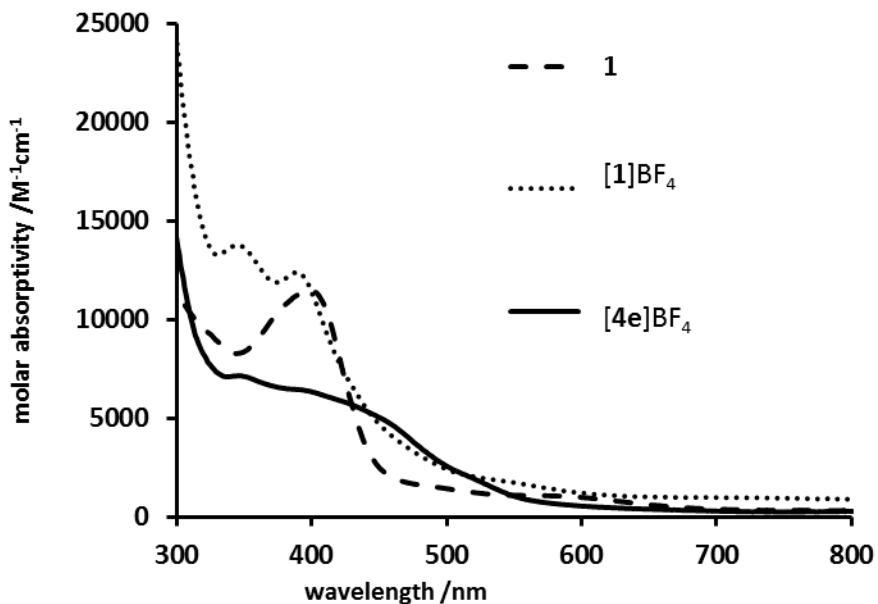


Figure S1: UV-vis spectra of **1**, $[1]BF_4$ and $[4e]BF_4$ (0.5 mM in CH_2Cl_2).

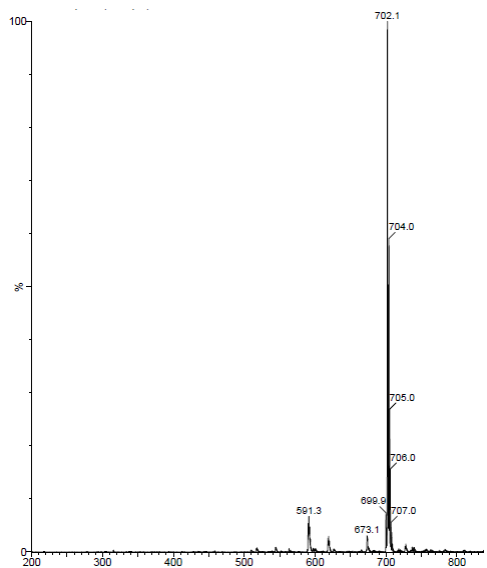


Figure S2: Positive ion ESI mass spectrum of $[1]\text{BF}_4$.

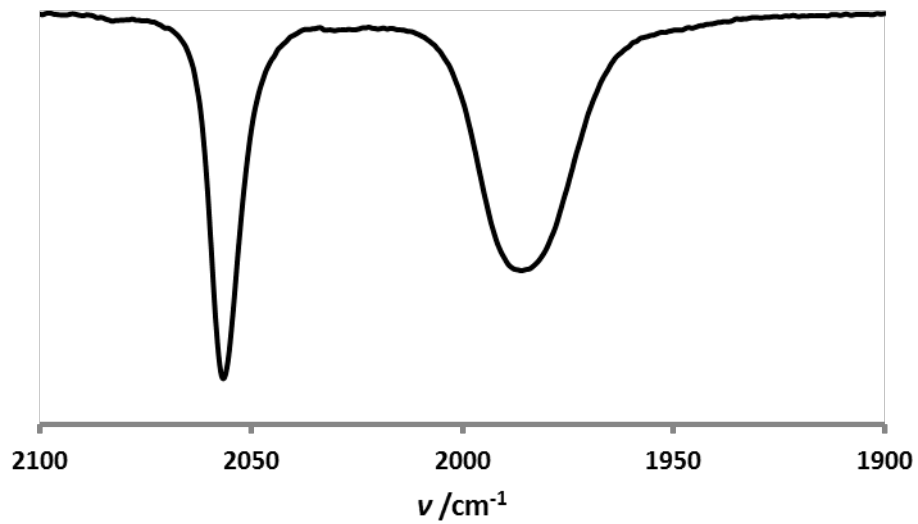


Figure S3: FT-IR spectrum (ν_{CO} region, CH_2Cl_2) of $[1]\text{BF}_4$.

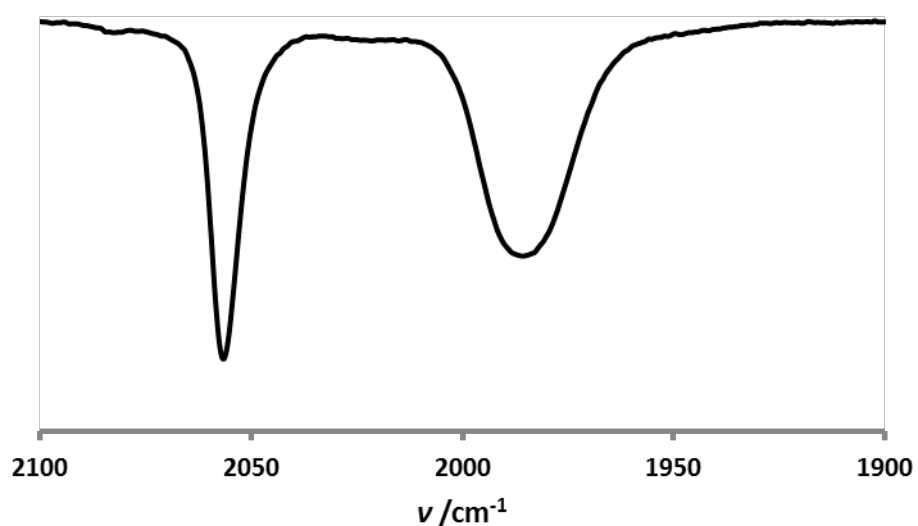


Figure S4: FT-IR spectrum (ν_{CO} region, CH_2Cl_2) of $[1]\text{PF}_6$.

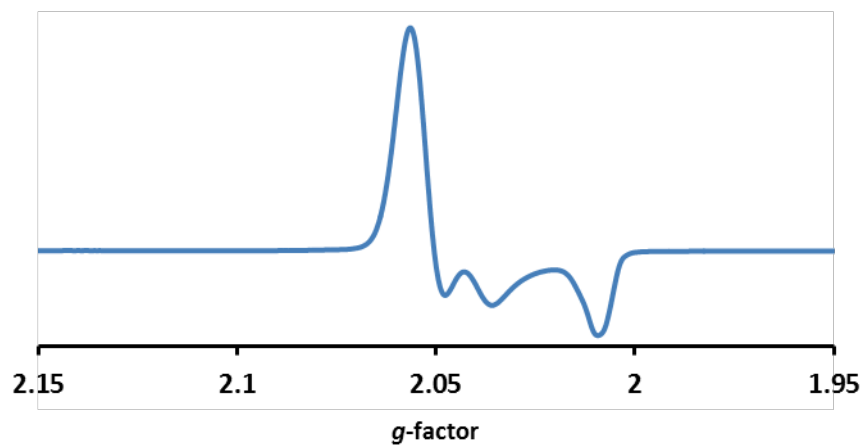


Figure S5: X-band EPR spectrum ($\text{CH}_2\text{Cl}_2/\text{PhMe}$, 110 K) of $[1]\text{PF}_6$.

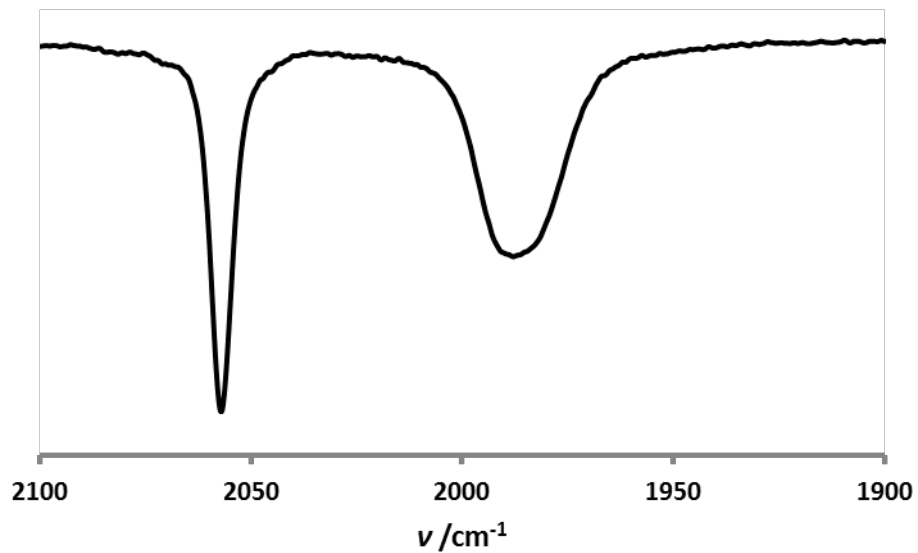


Figure S6: FT-IR spectrum (ν_{CO} region, CH_2Cl_2) of $[1]\text{BAr}_4^{\text{F}}$.

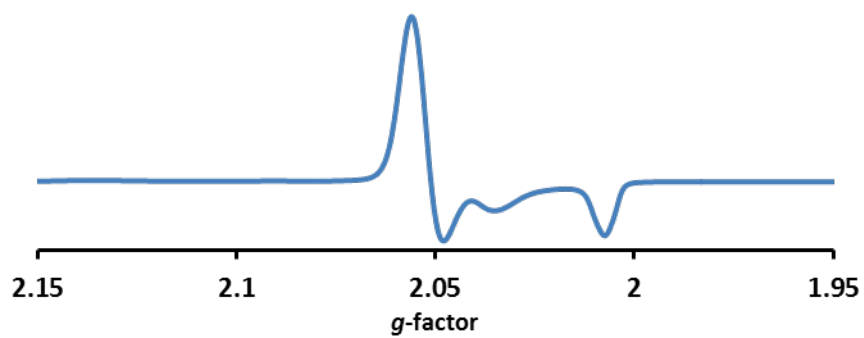


Figure S7: X-band EPR spectrum ($\text{CH}_2\text{Cl}_2/\text{PhMe}$, 110 K) of $[1]\text{BAr}_4^{\text{F}}$.

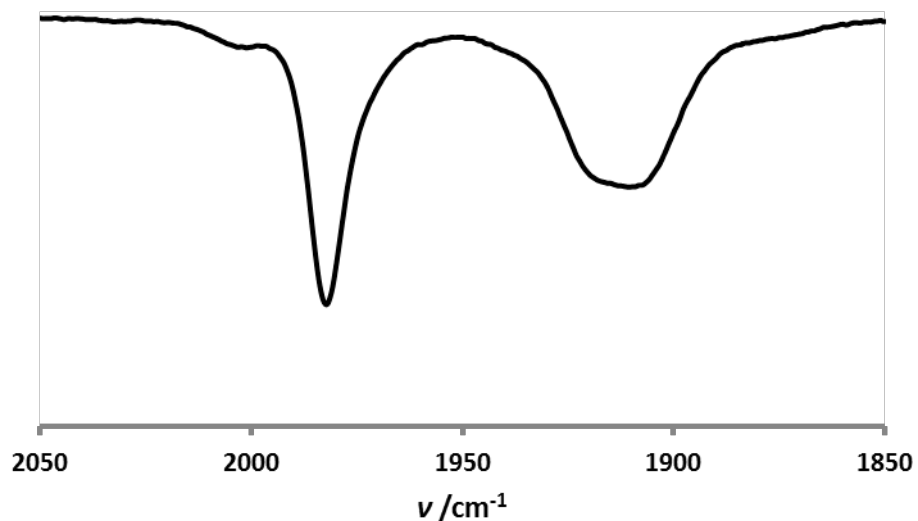


Figure S8: FT-IR spectrum (ν_{CO} region, CH_2Cl_2) of $[\mathbf{1}']$.

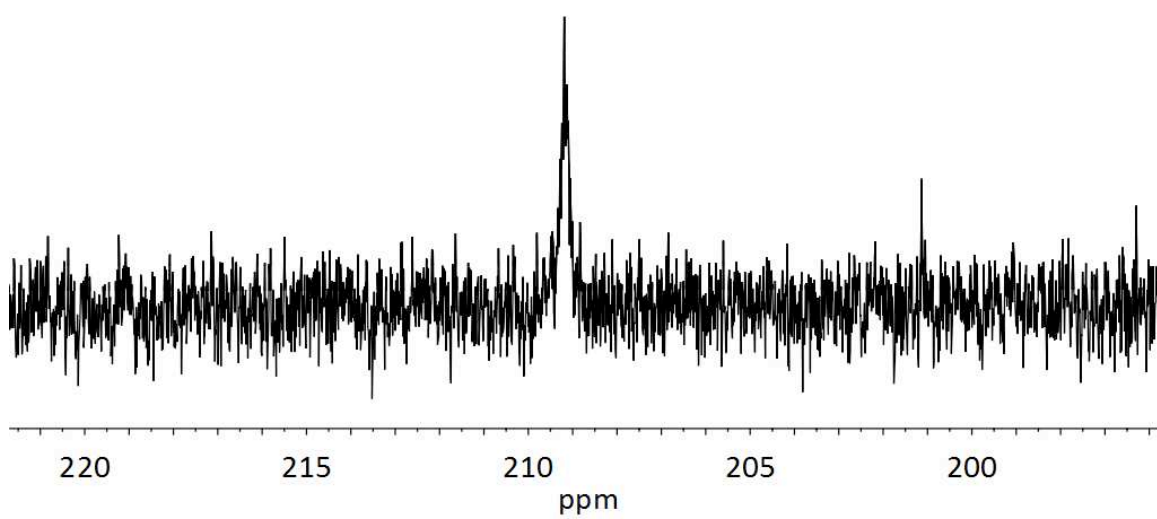


Figure S9: $^{13}\text{C}\{^1\text{H}\}$ NMR spectrum (CD_2Cl_2 , 202 MHz) of $[\mathbf{1}']$.

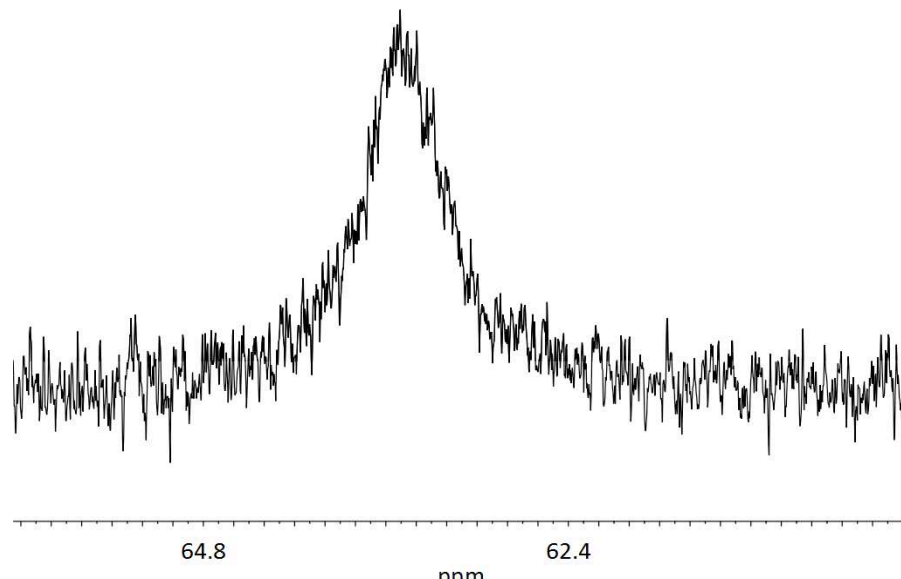


Figure S10: $^{31}\text{P}\{\text{H}\}$ NMR spectrum (CD_2Cl_2 , 202 MHz) of $[1']$.

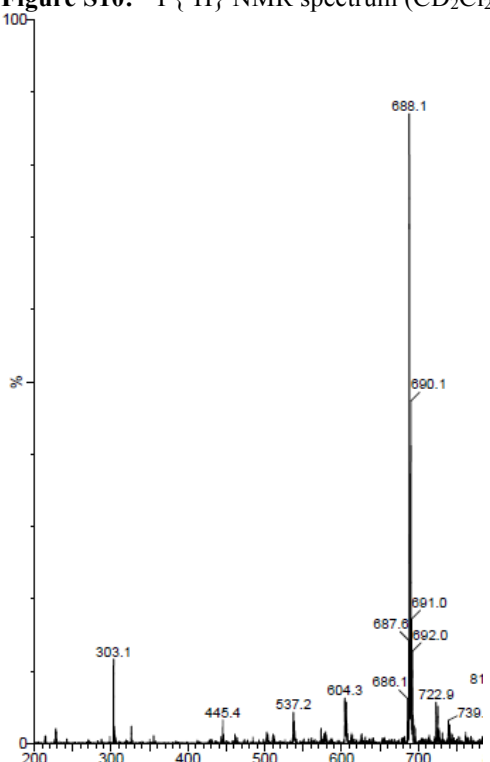


Figure S11: Positive ion ESI mass spectrum of $[2]\text{BF}_4$.

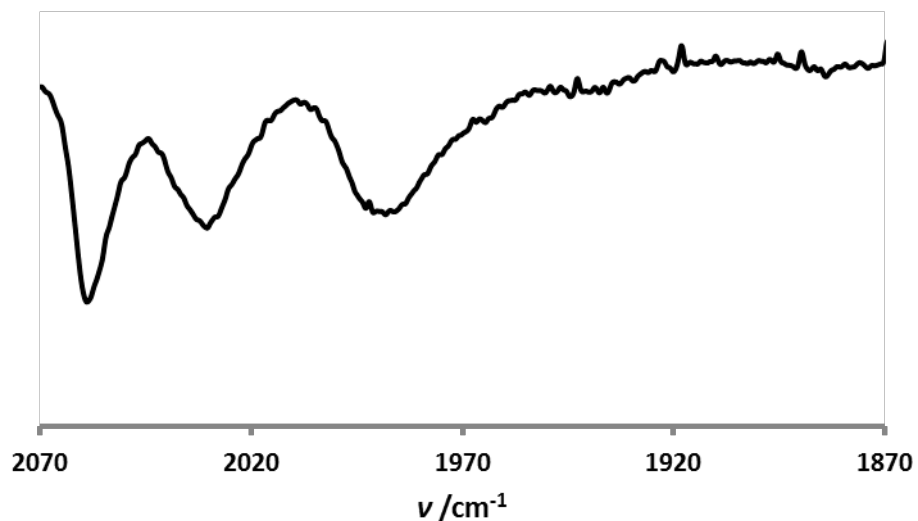


Figure S12: FT-IR spectrum (ν_{CO} region, CH_2Cl_2) of $[2]\text{BF}_4$.

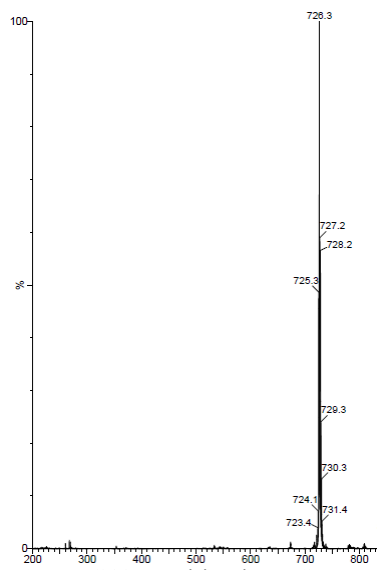


Figure S13: Positive ion ESI mass spectrum of $[3]\text{BF}_4$.

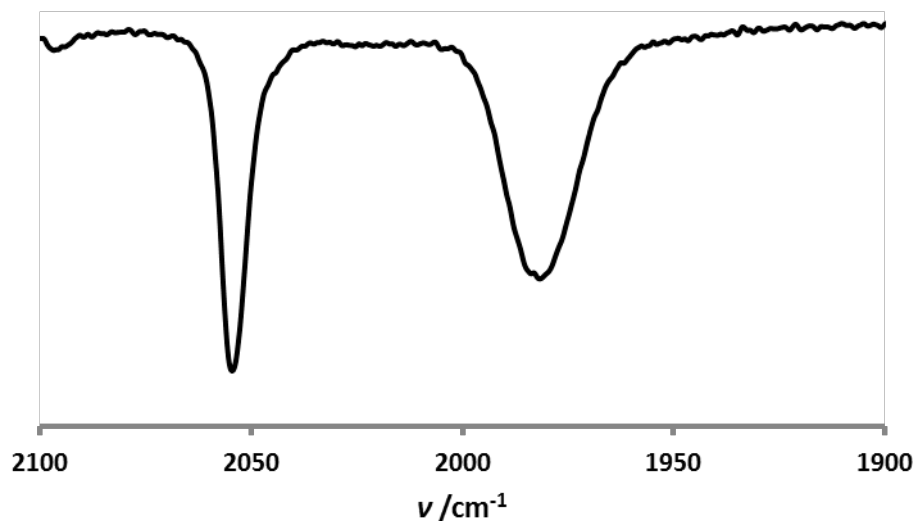


Figure S14: FT-IR spectrum (ν_{CO} region, CH_2Cl_2) of $[3]\text{BF}_4$.

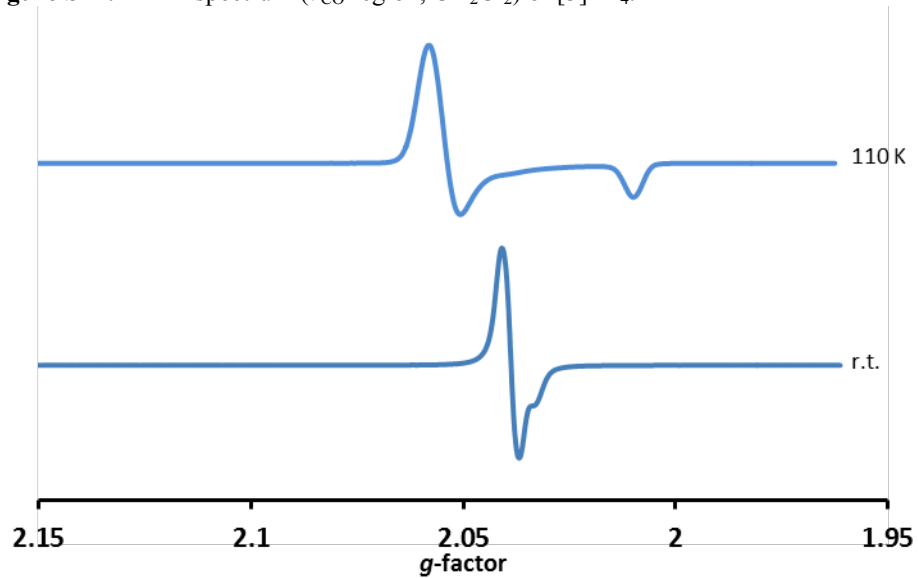


Figure S15: X-band EPR spectra ($\text{CH}_2\text{Cl}_2/\text{PhMe}$) of $[3]\text{BF}_4$ at 110 K and room temperature.

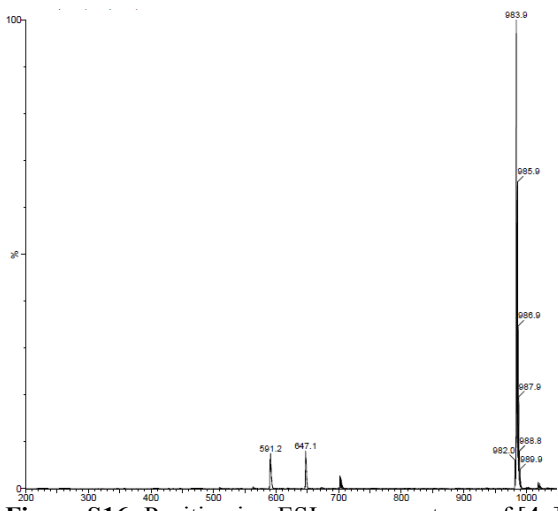


Figure S16: Positive ion ESI mass spectrum of $[4\text{a}]\text{BF}_4$.

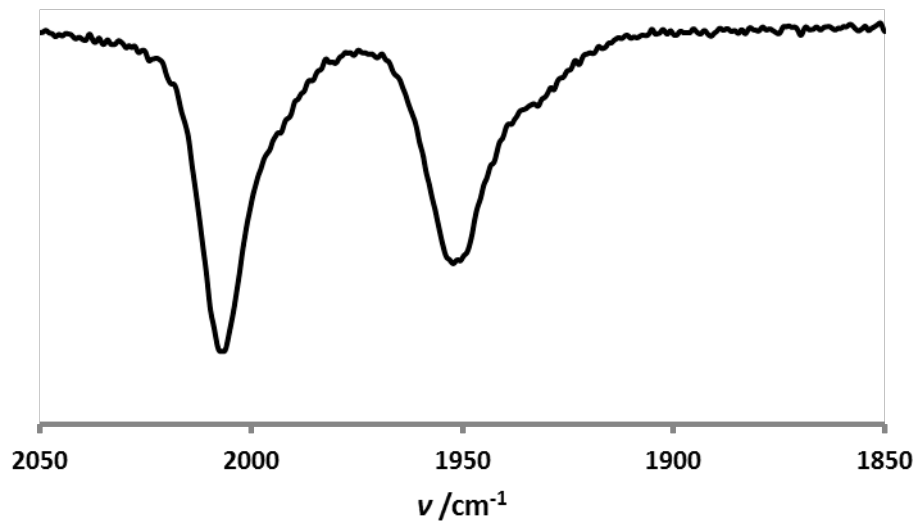


Figure S17: FT-IR spectrum (v_{CO} region, CH_2Cl_2) of $[4\text{a}]\text{BF}_4$.

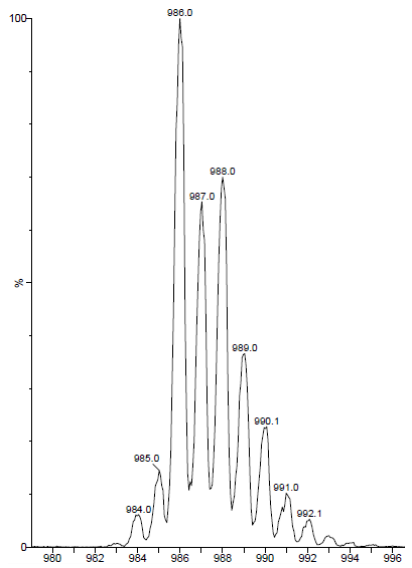


Figure S18: Positive ion ESI mass spectrum of [4a']BF₄.

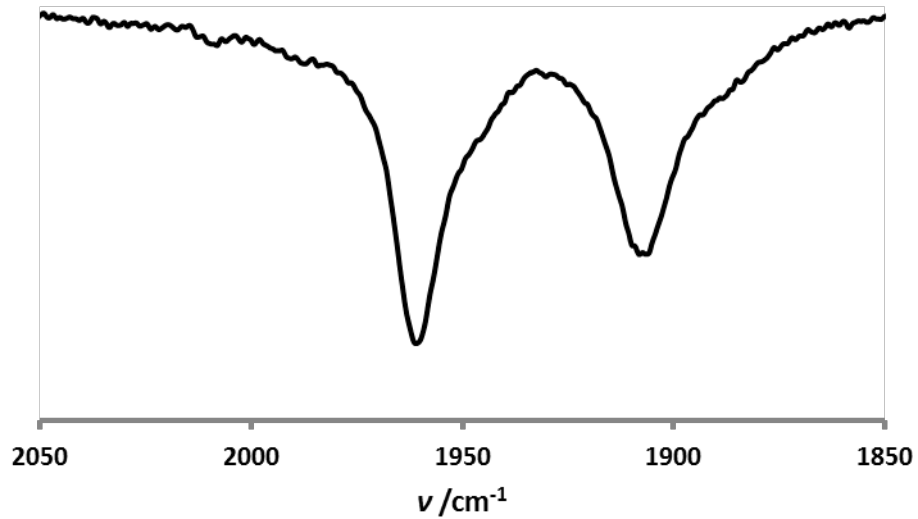


Figure S19: FT-IR spectrum (ν_{CO} region, CH₂Cl₂) of [4a']BF₄.

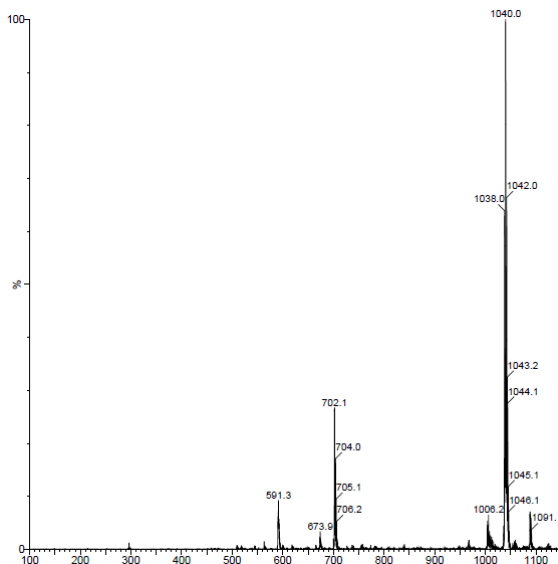


Figure S20: Positive ion ESI mass spectrum of $[4b]BF_4$.

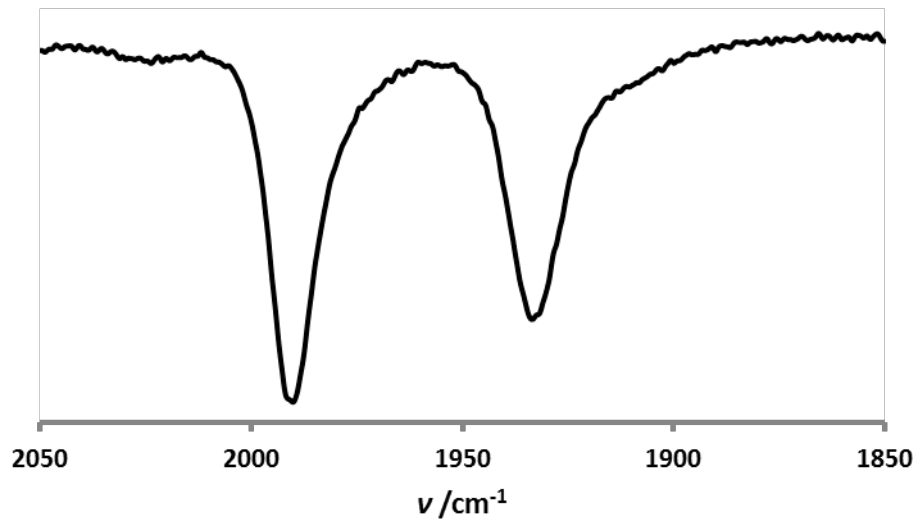


Figure S21: FT-IR spectrum (ν_{CO} region, CH_2Cl_2) of $[4b]BF_4$.

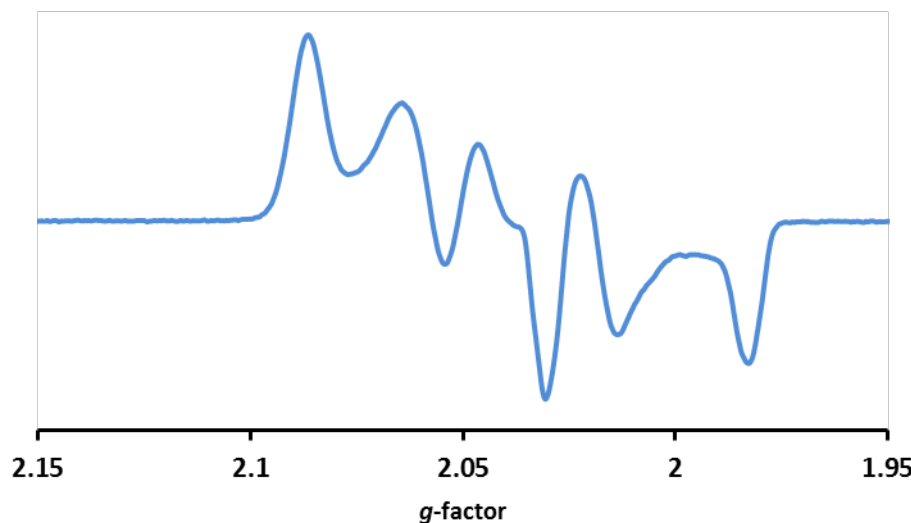


Figure S22: X-band EPR spectrum ($\text{CH}_2\text{Cl}_2/\text{PhMe}$, 110 K) of $[4\mathbf{b}]\text{BF}_4$.

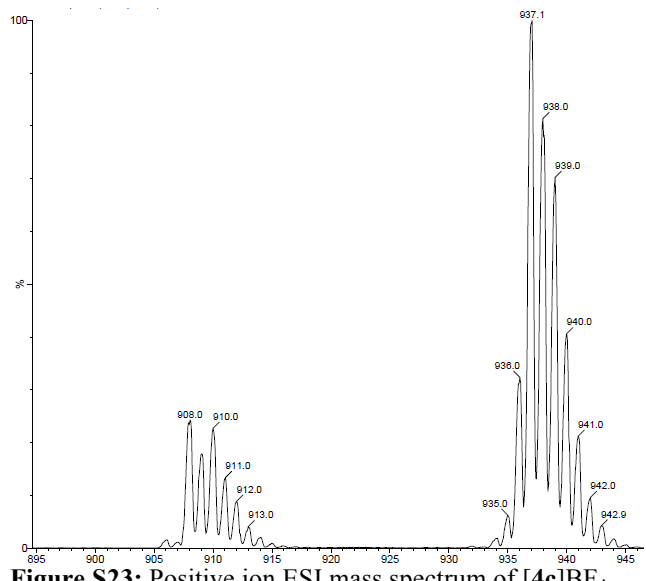


Figure S23: Positive ion ESI mass spectrum of $[4\mathbf{c}]\text{BF}_4$.

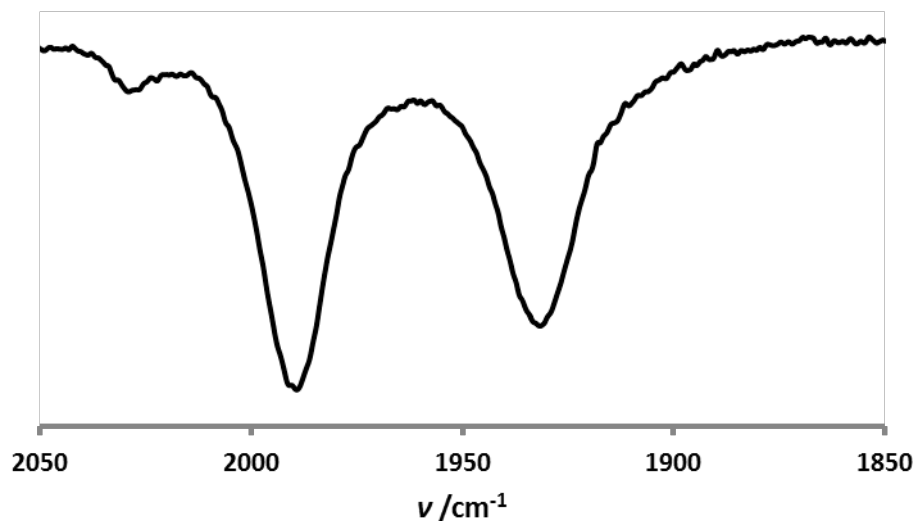


Figure S24: FT-IR spectrum (ν_{CO} region, CH_2Cl_2) of $[4\mathbf{c}]\text{BF}_4$.

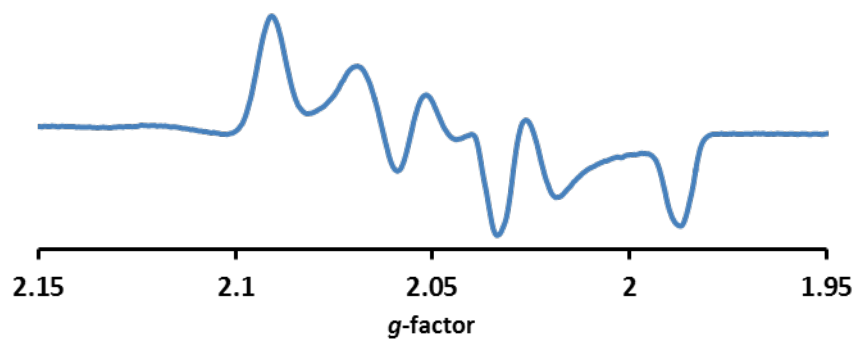


Figure S25: X-band EPR spectrum ($\text{CH}_2\text{Cl}_2/\text{PhMe}$, 110 K) of $[4\mathbf{c}]\text{BF}_4$.

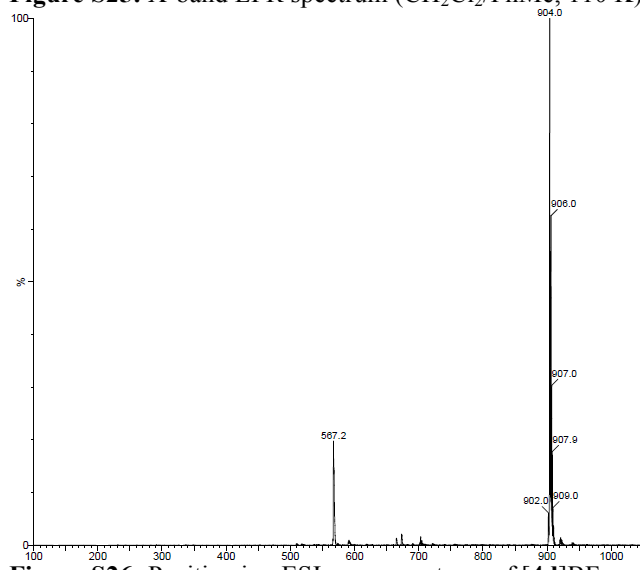


Figure S26: Positive ion ESI mass spectrum of $[4\mathbf{d}]\text{BF}_4$.

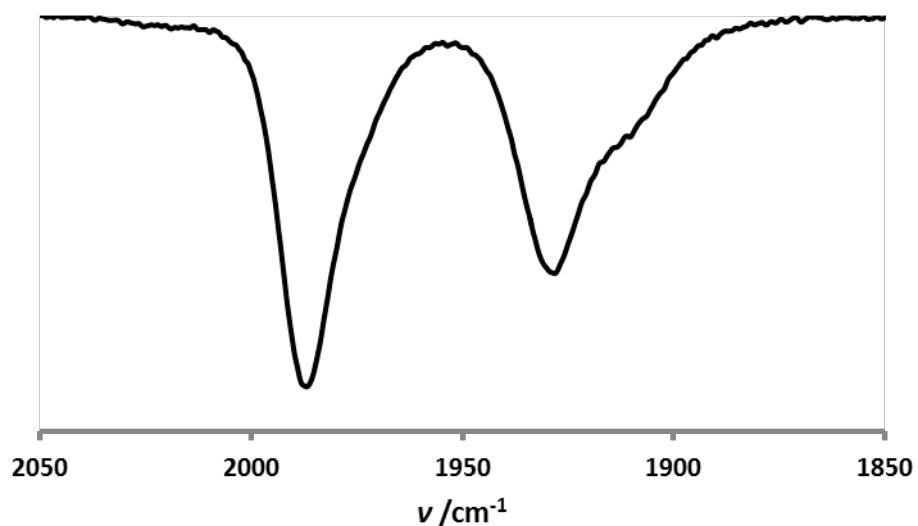


Figure S27: FT-IR spectrum (v_{CO} region, CH_2Cl_2) of $[4\mathbf{d}]\text{BF}_4$.

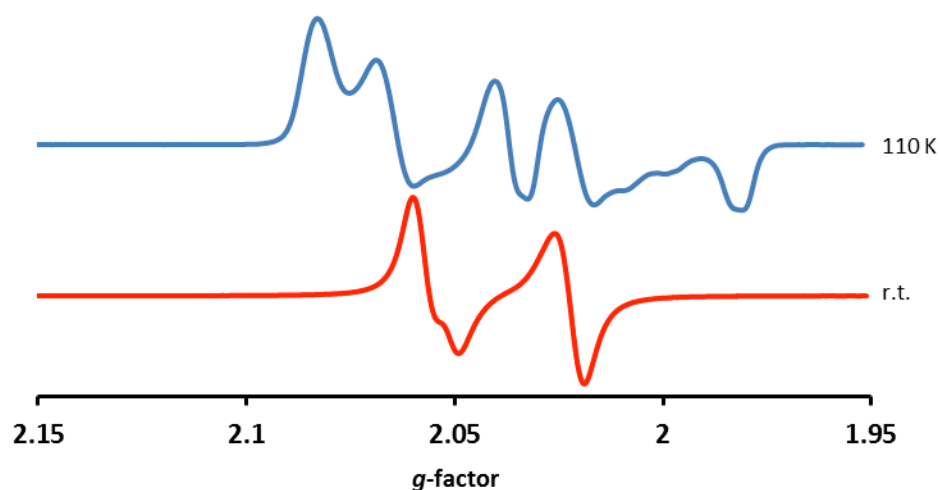


Figure S28: X-band EPR spectra ($\text{CH}_2\text{Cl}_2/\text{PhMe}$) of $[4\mathbf{d}]\text{BF}_4$ collected at 110 K and room temperature.

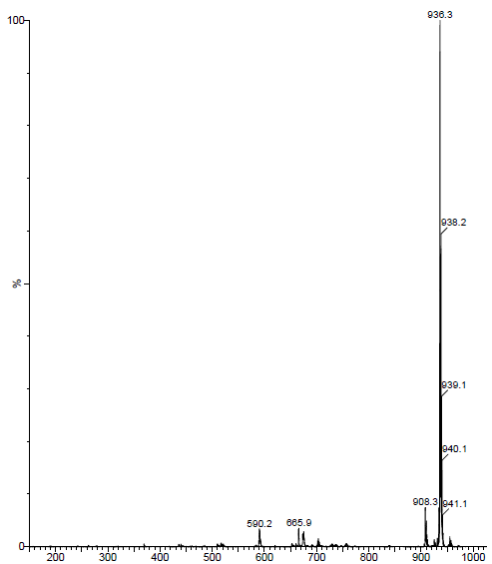


Figure S29: Positive ion ESI mass spectrum of [4e]BF₄.

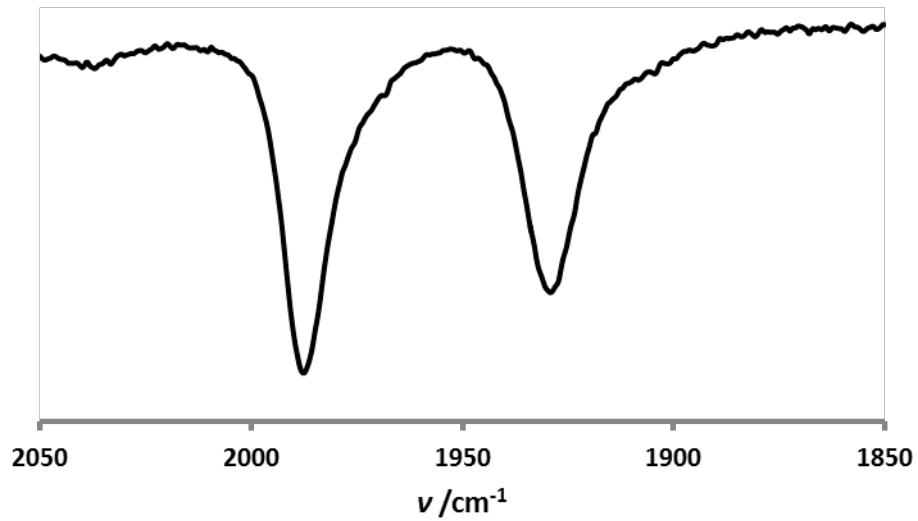


Figure S30: FT-IR spectrum (ν_{CO} region, CH₂Cl₂) of [4e]BF₄.

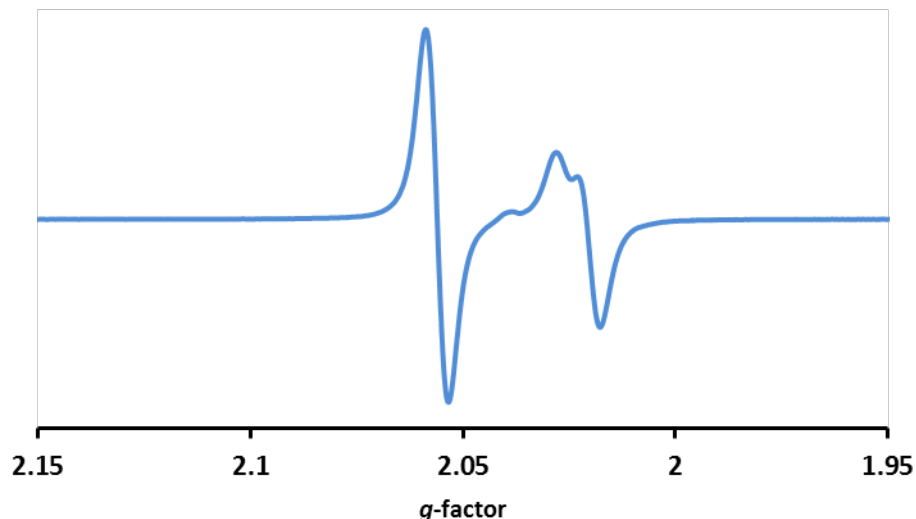


Figure S31: X-band EPR spectrum ($\text{CH}_2\text{Cl}_2/\text{PhMe}$, rt) of $[4\text{e}]\text{BF}_4$.

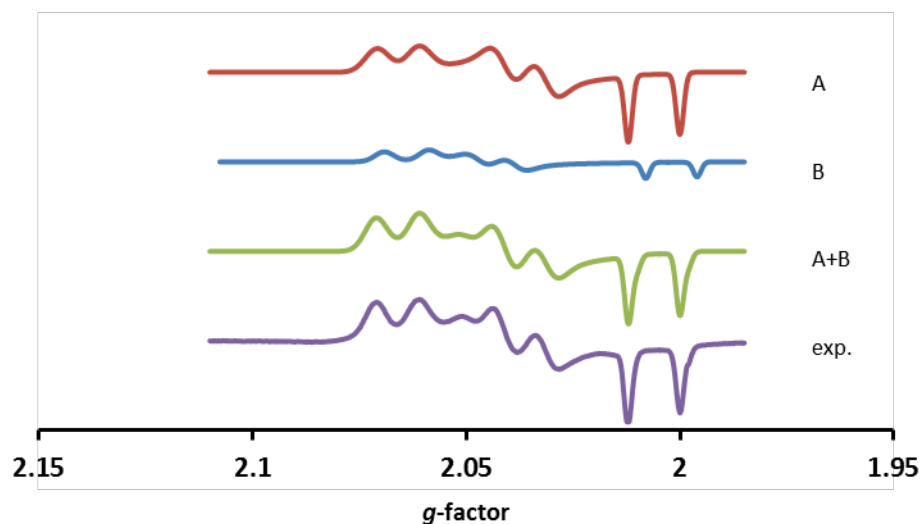


Figure S32: Q-band EPR spectra ($\text{CH}_2\text{Cl}_2/\text{PhMe}$, 130 K) of $[4\text{e}]\text{BF}_4$. The experimental spectrum could be simulated as a sum of two components, denoted A and B.

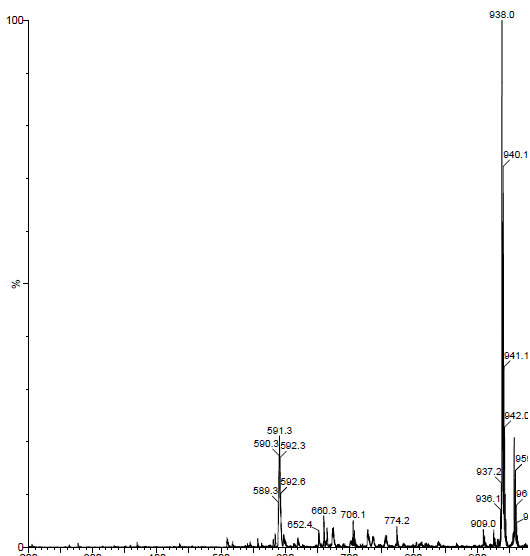


Figure S33: Positive ion ESI mass spectrum of $[4e']\text{BF}_4$.

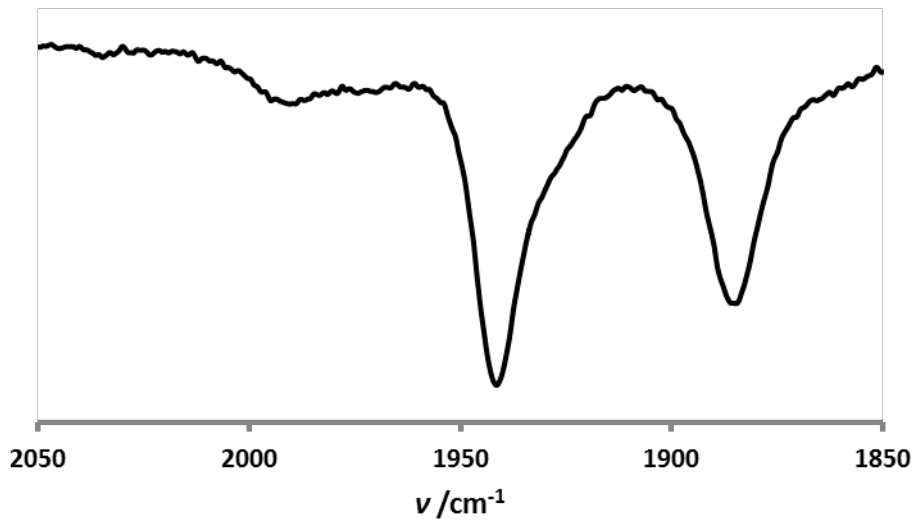


Figure S34: FT-IR spectrum (ν_{CO} region, CH_2Cl_2) of $[4e']\text{BF}_4$.

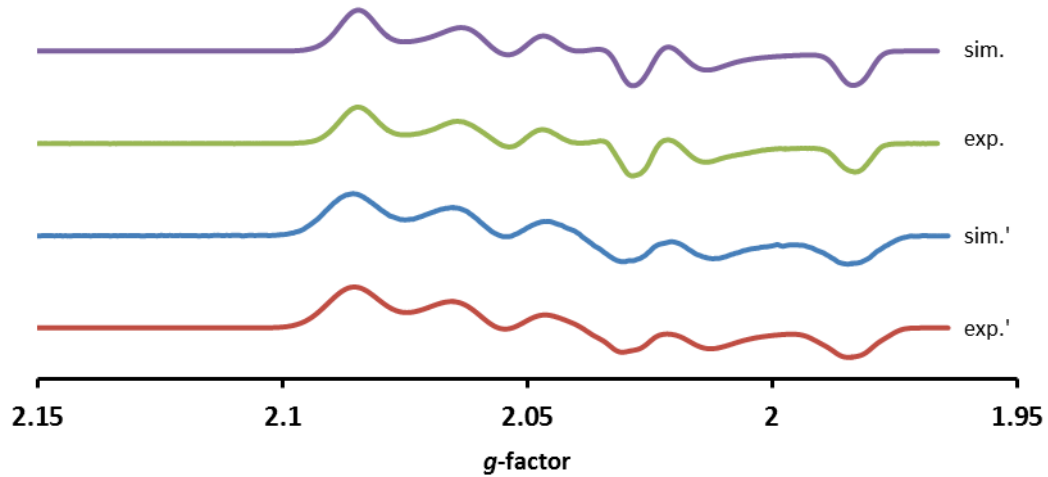


Figure S35: X-band EPR spectrum ($\text{CH}_2\text{Cl}_2/\text{PhMe}$, 110 K) of $[4\mathbf{e}]\text{BF}_4$ (exp.) and $[4\mathbf{e}']\text{BF}_4$ (exp.'), along with their simulated spectra (sim. and sim.', respectively).

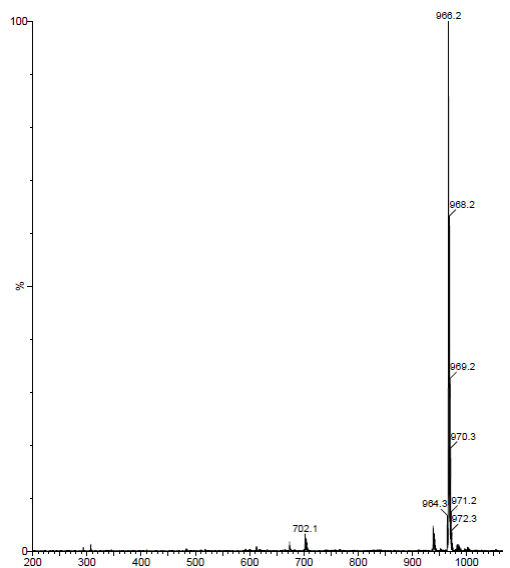


Figure S36: Positive ion ESI mass spectrum of $[4\mathbf{f}]\text{BF}_4$.

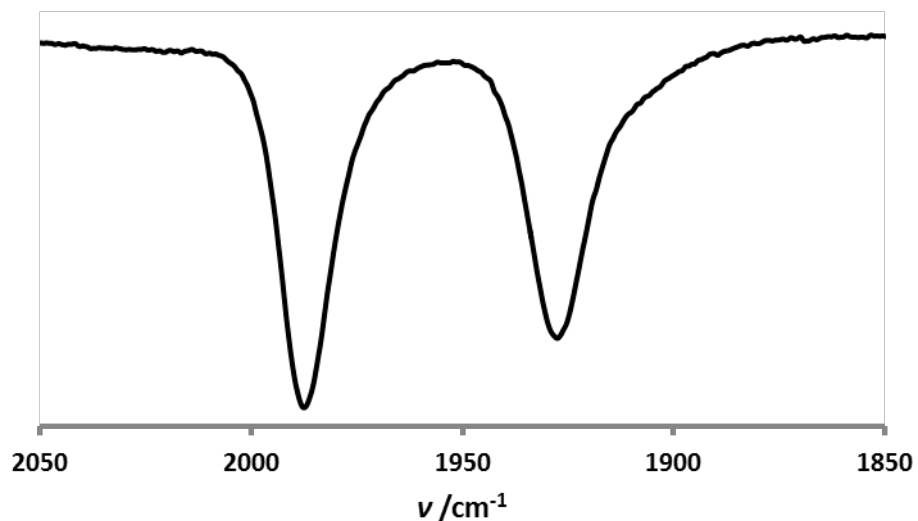


Figure S37: FT-IR spectrum (ν_{CO} region, CH_2Cl_2) of $[4\mathbf{f}]\text{BF}_4$.

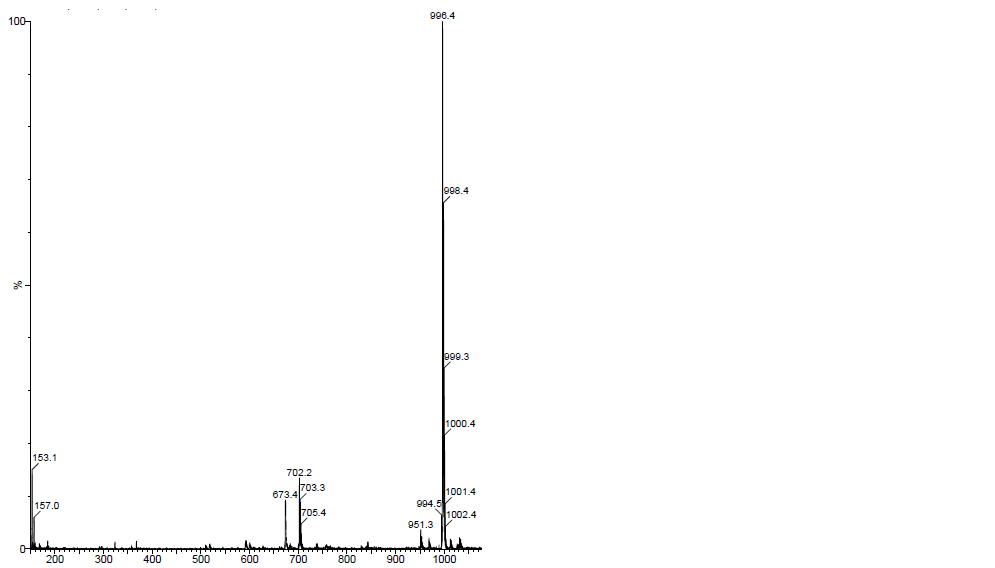


Figure S38: Positive ion ESI mass spectrum of $[4\mathbf{g}]\text{BF}_4$.

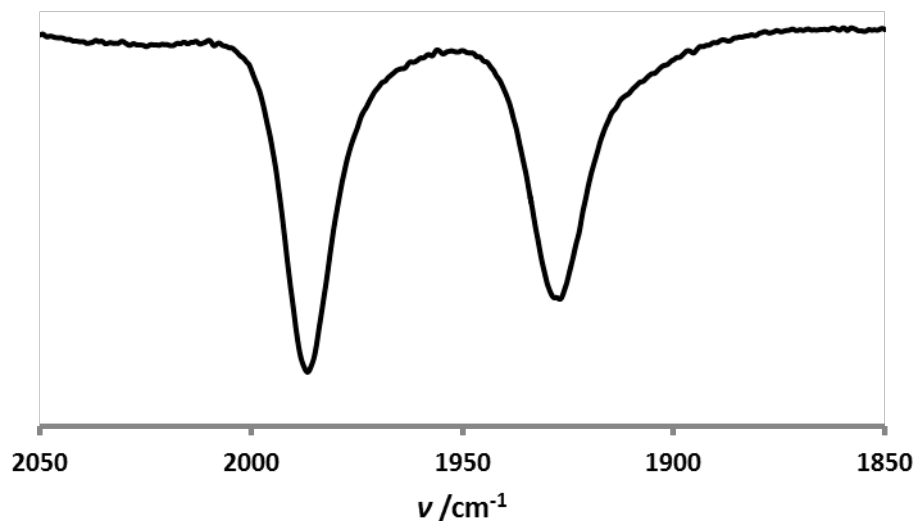


Figure S39: FT-IR spectrum (ν_{CO} region, CH_2Cl_2) of **[4g]** BF_4 .

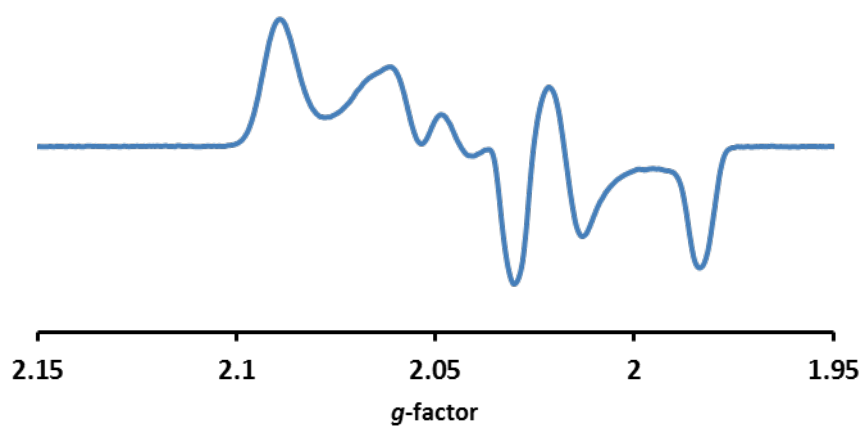


Figure S40: X-band EPR spectrum ($\text{CH}_2\text{Cl}_2/\text{PhMe}$, 110 K) of **[4g]** BF_4 .

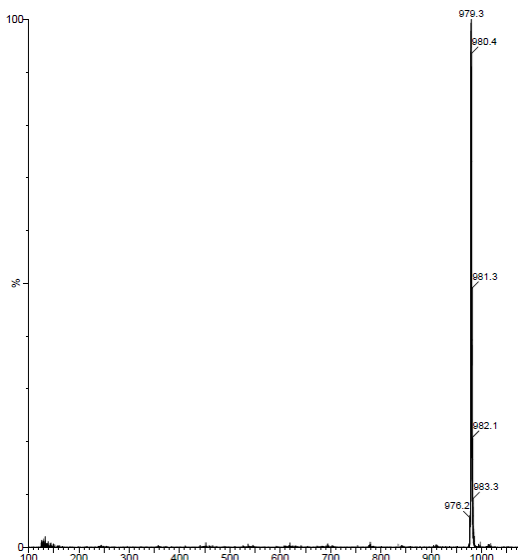


Figure S41: Positive ion ESI mass spectrum of **[4h]BF₄**.

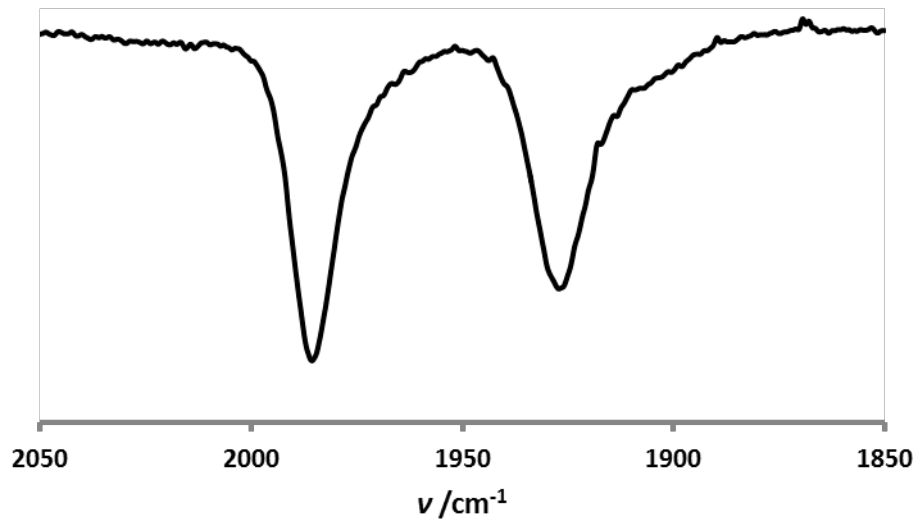


Figure S42: FT-IR spectrum (ν_{CO} region, CH_2Cl_2) of **[4h]BF₄**.

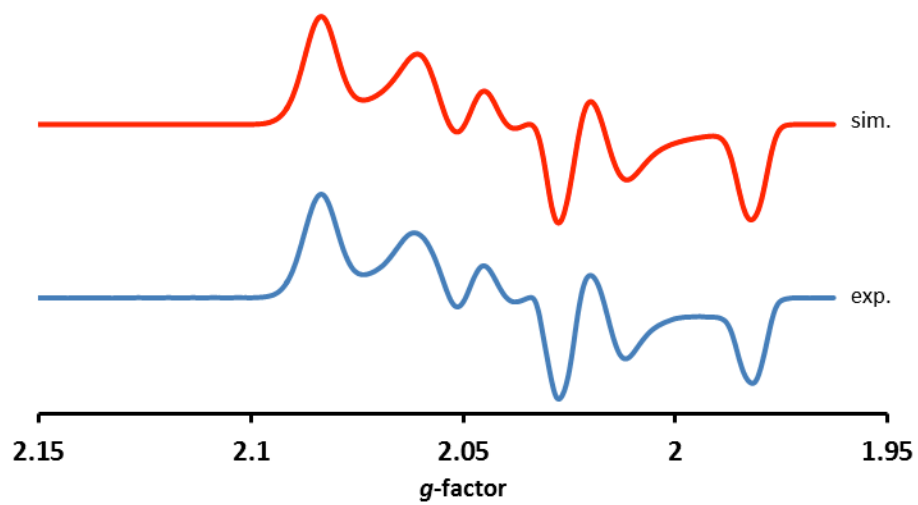


Figure S43: The simulated and experimental X-band EPR spectrum ($\text{CH}_2\text{Cl}_2/\text{PhMe}$, 110 K) of **[4h]BF₄**.

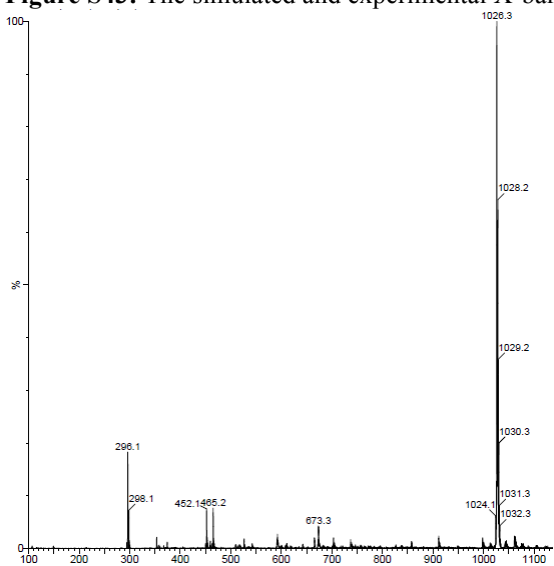


Figure S44: Positive ion ESI mass spectrum of **[4i]BF₄**.

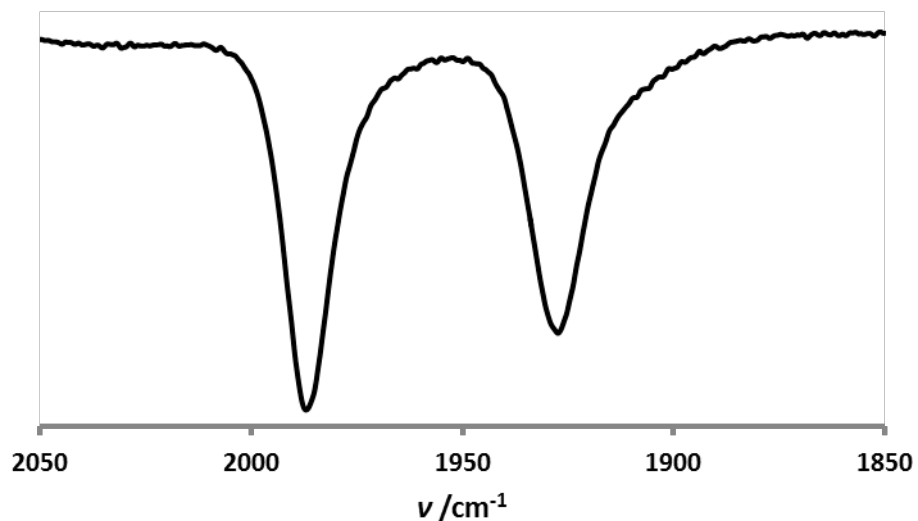


Figure S45: FT-IR spectrum (ν_{CO} region, CH_2Cl_2) of **[4i]** BF_4 .

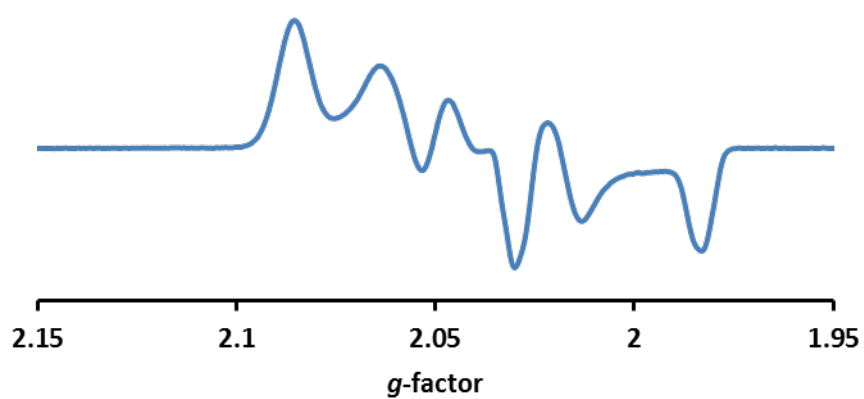


Figure S46: X-band EPR spectrum ($\text{CH}_2\text{Cl}_2/\text{PhMe}$, 110 K) of **[4i]** BF_4 .

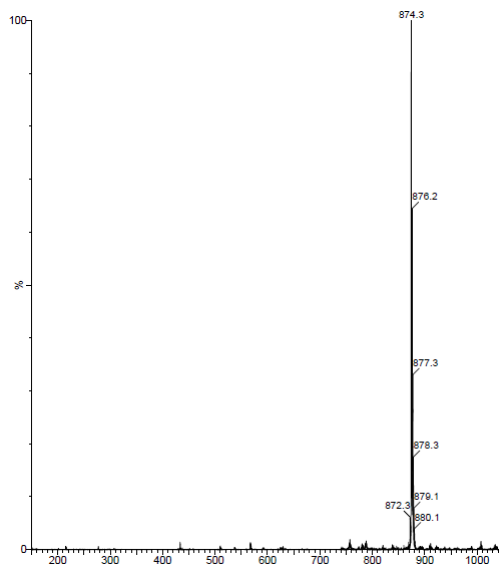


Figure S47: Positive ion ESI mass spectrum of [4j]BF₄.

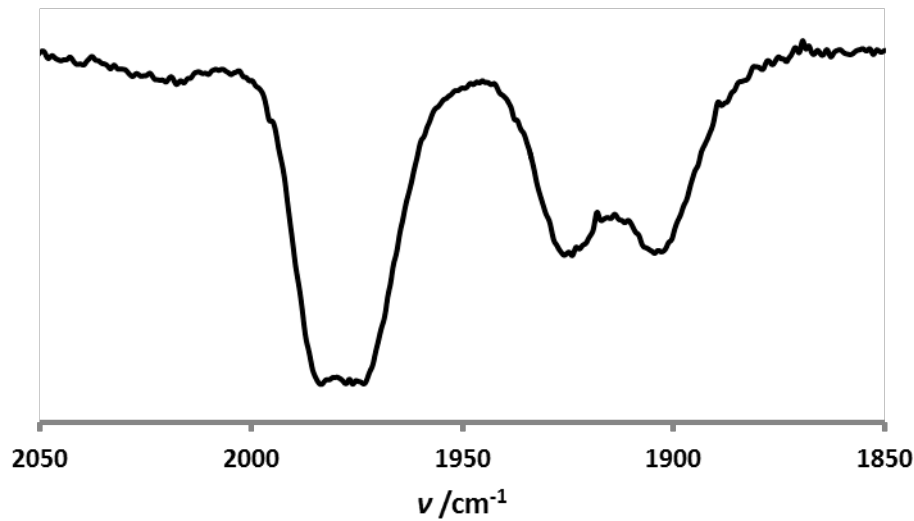


Figure S48: FT-IR spectrum (ν_{CO} region, CH₂Cl₂) of [4j]BF₄.

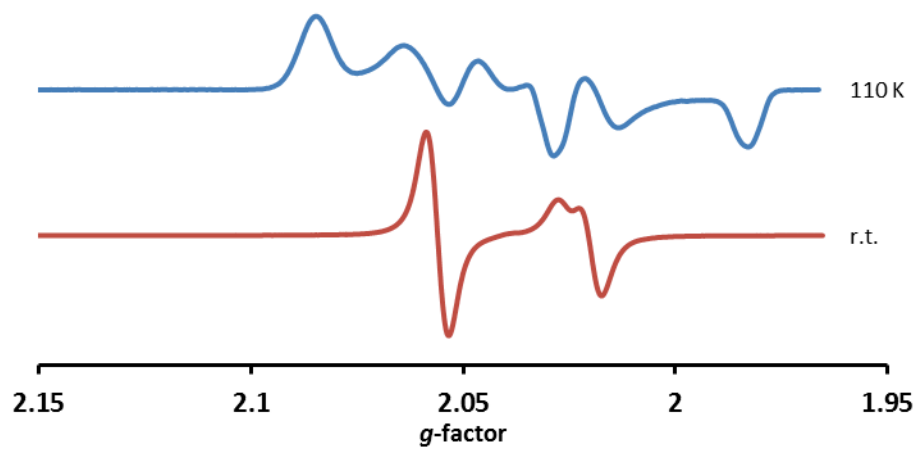


Figure S49: X-band EPR spectra ($\text{CH}_2\text{Cl}_2/\text{PhMe}$) of **[4j]** BF_4 collected at 110 K and room temperature.

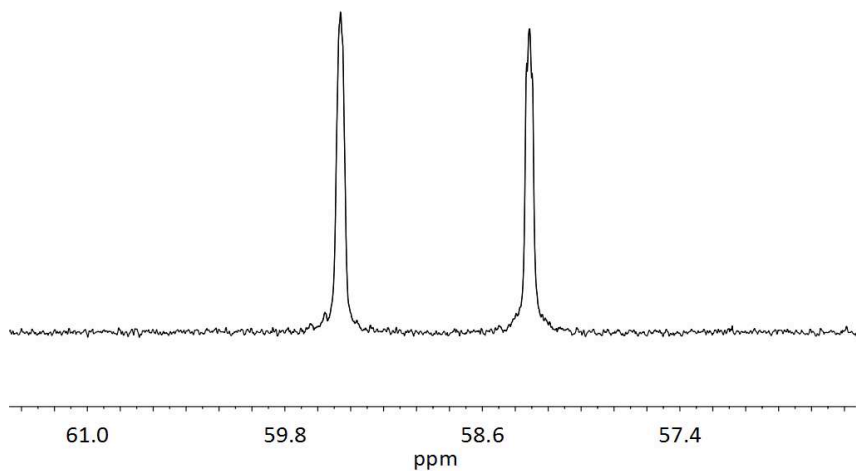


Figure S50: $^{31}\text{P}\{\text{H}\}$ NMR spectrum (CD_2Cl_2 , 202 MHz) of **[5]** $(\text{BF}_4)_2$.

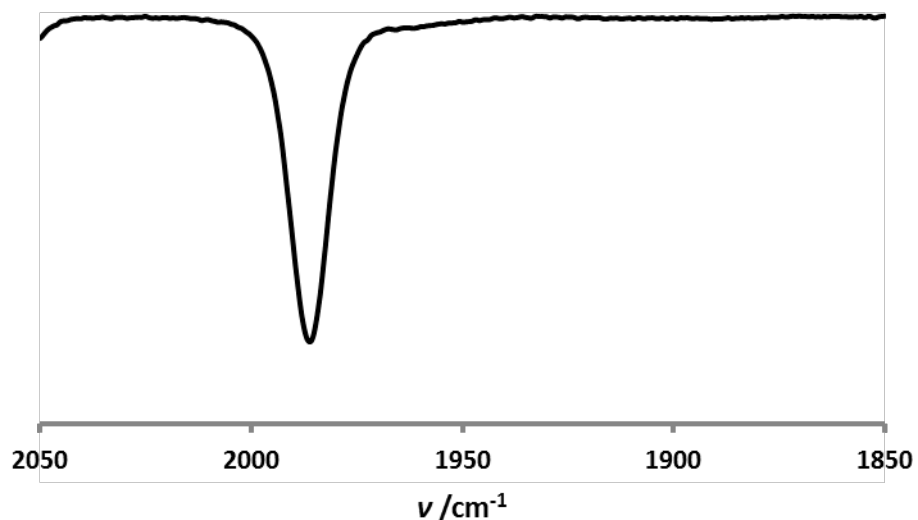


Figure S51: FT-IR spectrum (v_{CO} region, CH_2Cl_2) of **[5]** $(\text{BF}_4)_2$.

Table 1: Calculated g-tensor principal values for complexes $[1]^+$, $[2]^+$, $[3]^+$, $[4a]^+$ and $[4e]^+$ (superscripts ^a and ^b refer to flipamers of each complex, see Scheme 5).

Complex	SOMF(1X) TZVP <i>g</i> ₁ , <i>g</i> ₂ , <i>g</i> ₃			ZORA SO ROKS DZ <i>g</i> ₁ , <i>g</i> ₂ , <i>g</i> ₃		
	BP	B3LYP	PBE0	BP	B3LYP	PBE0
	2.033, 2.030, 2.012	2.044, 2.042, 2.005	2.047, 2.044, 2.004	2.041, 2.035, 2.020	2.052, 2.051, 2.006	2.057, 2.055, 2.004
$[1]^{+a}$	2.033, 2.027, 2.012	2.044, 2.037, 2.004	2.047, 2.038, 2.003	2.042, 2.030, 2.019	2.051, 2.047, 2.005	2.055, 2.051, 2.004
	2.029, 2.026, 2.011	2.041, 2.038, 2.004	2.044, 2.040, 2.003	2.037, 2.029, 2.010	2.049, 2.044, 2.008	2.055, 2.048, 2.003
	2.033, 2.030, 2.016	2.045, 2.041, 2.006	2.048, 2.044, 2.005	2.043, 2.035, 2.026	2.052, 2.047, 2.010	2.057, 2.051, 2.008
$[3]^{+b}$	2.033, 2.027, 2.013	2.041, 2.038, 2.004	2.044, 2.040, 2.004	2.042, 2.029, 2.024	2.048, 2.047, 2.008	2.052, 2.051, 2.006
	2.038, 2.025, 2.014	2.061, 2.037, 2.010	2.065, 2.038, 2.011	2.045, 2.029, 2.018	2.060, 2.043, 2.006	2.065, 2.046, 2.004
	2.044, 2.026, 2.006	2.064, 2.047, 2.003	2.069, 2.048, 2.003	2.057, 2.024, 2.002	2.072, 2.057, 1.996	2.080, 2.065, 1.993
$[4a]^{+a}$	2.045, 2.032, 2.007	2.067, 2.053, 2.004	2.072, 2.056, 2.004	2.059, 2.038, 2.006	2.074, 2.067, 1.997	2.082, 2.076, 1.994
	2.043, 2.026, 2.006	2.064, 2.047, 2.003	2.068, 2.048, 2.003	2.057, 2.024, 2.002	2.072, 2.057, 1.996	2.080, 2.065, 1.993

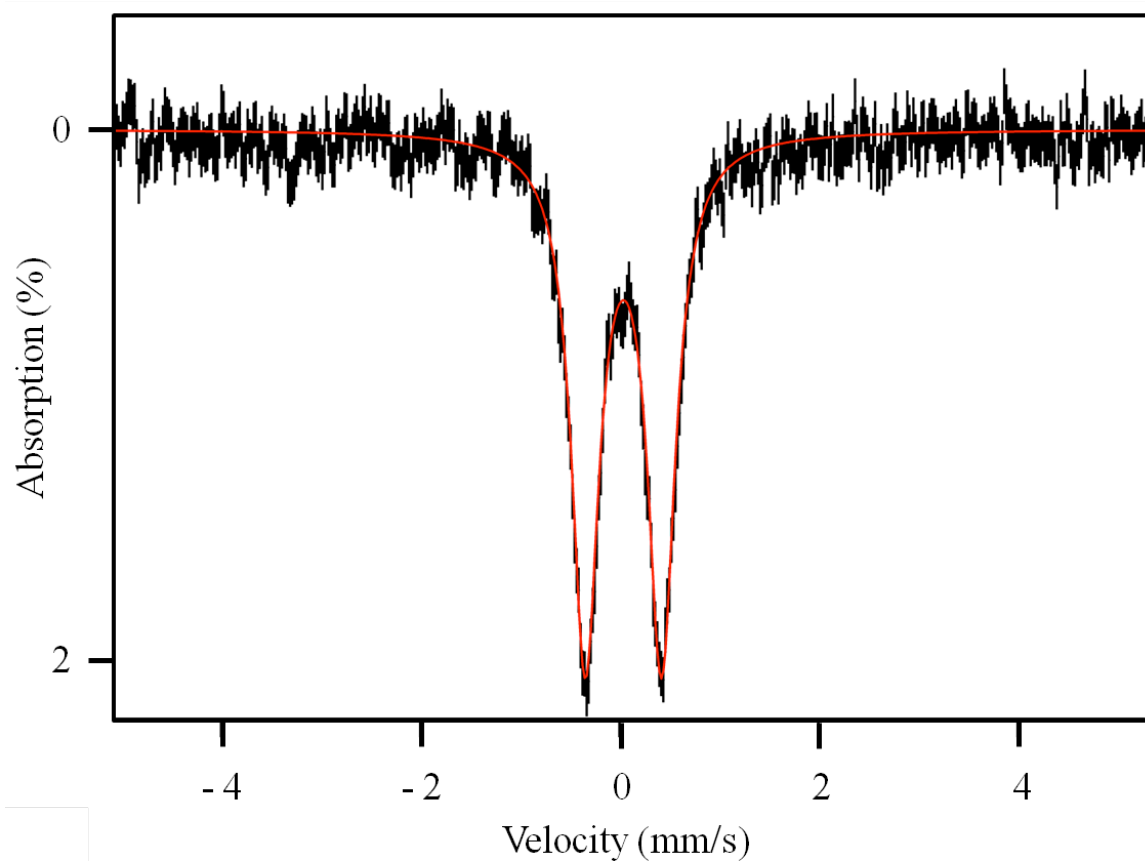


Figure S52: Mössbauer spectrum (5 K, 500 G) of $(CO)_3Fe(pdt)Fe(CO)_3$, and simulated spectrum (solid trace).

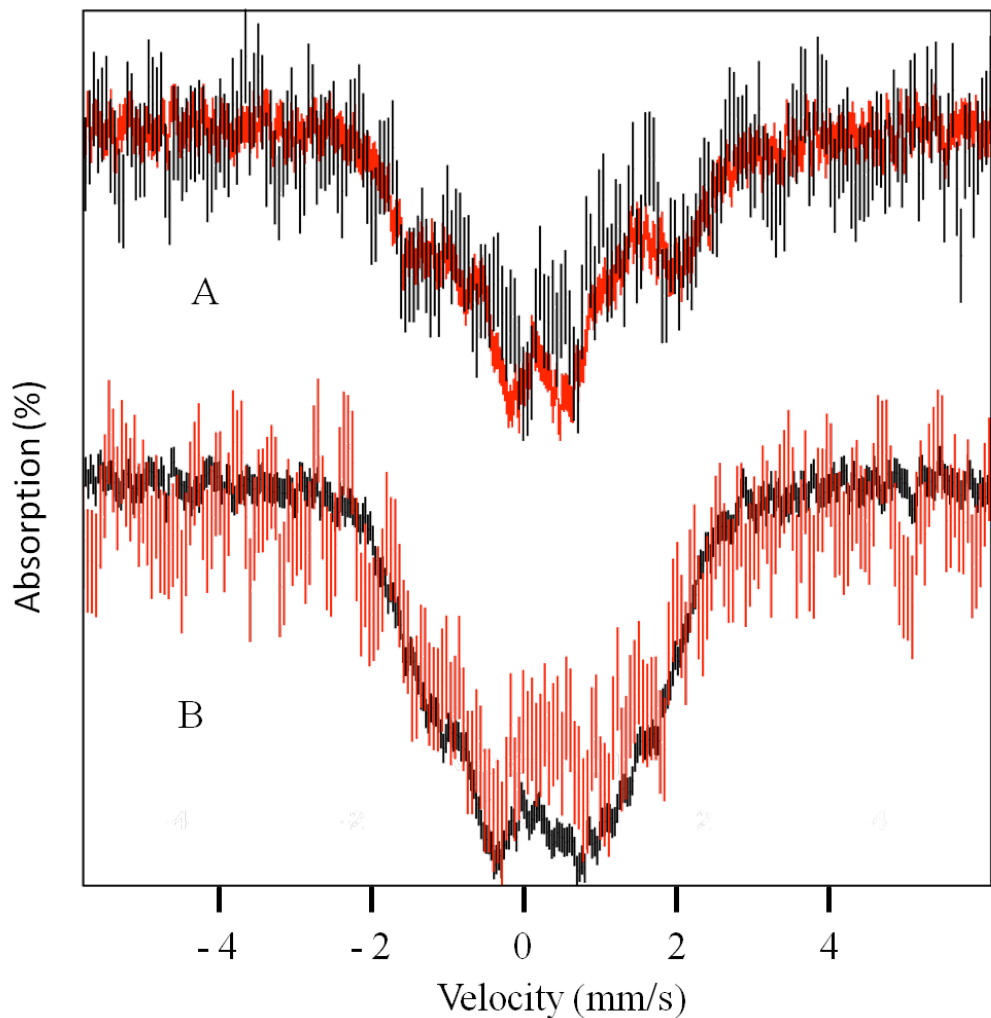


Figure S53: Mössbauer spectra of **[4e]BF₄**. A: 5 K, 500 G, 5 mM sample spectrum (black) overlaid on 40 mM sample spectrum (red). B: 4.2 K, 6 T Mössbauer data for **[4e]BF₄**, solid sample spectrum (black) overlaid on 40 mM sample spectrum (red).